2024-05-15

Assessing the impact of an offshore longline mussel farm on local water circulation in a highly hydrodynamic energetic bay

Mascorda-Cabre, L

10.1016/j.aquaculture.2024.740697
Aquaculture
Elsevier BV

Aquaculture 585 (2024) 740697

Contents lists available at ScienceDirect

Aquaculture

journal homepage: www.elsevier.com/locate/aquaculture

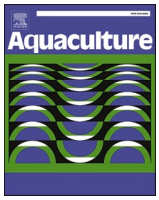

Assessing the impact of an offshore longline mussel farm on local water circulation in a highly hydrodynamic energetic bay

Llucia Mascorda-Cabre *, Emma V. Sheehan, Martin J. Attrill, Phil Hosegood

School of Biological and Marine Sciences, Faculty of Science and Engineering, University of Plymouth, Plymouth, UK

ARTICLE INFO

Keywords:
Mussel farm
Offshore aquaculture
Hydrodynamic flow
Currents
ADCP

ABSTRACT

Thought to be a sustainable choice, molluscs are the most consumed aquaculture foods after finfish. The expansion of the mussel aquaculture industry offshore reports lower environmental impacts compared to inshore farms. Although an offshore location has the potential to reduce a farm's ecological impacts, the effect of large developments on water currents is still not fully understood. High hydrodynamic regimes can influence the dispersion of farm biodeposits, organic loading, flow alterations with the potential to impact water residence time, particle and sediment dispersal (including larvae and biodeposits) and seabed sediment resuspension, which in turn, can have ecological impacts. Farm-induced flow changes of the UK's first large scale suspended longline mussel farm were assessed by a combination of oceanographic mooring and vessel-mounted Acoustic Doppler Current Profiler (ADCP) measurements. Data was separated by upstream and downstream according to the direction of the flow in relation to the farm. M-ADCP results showed a 28% decrease current velocities within the farm's boundaries, demonstrating within-farm current attenuation produced by mussel ropes drag. Flow was then redistributed above and beneath the farm showing velocity increases of 66% and 7% respectively, resulting in above-farm flow acceleration and downwelling (with up to 171% increase in near-seabed velocities compared to sea surface velocities). However, overall mean downstream sea surface velocities decreased by 63%. An overall 21% increase in near-seabed velocities showed the farm's effect on near-bed currents, the opposite to what is naturally achieved by seabed friction. This was further measured by VM-ADCP results also showing secondary flow acceleration at the farm's flanks and increased near-headline flow perturbations of up to 80% mean u velocities over a small horizontal scale (0.5 km), further demonstrating the effects of the farm on the local circulation. Through-farm surface current velocities (waves) were reduced by up to 72%. Flow changes were localised and dependent on the different tidal phases, the farm's design and, the abundance of mussel ropes providing drag.

1. Introduction

With the intensification of shellfish farming in inshore locations, a range of factors limit its expansion: space usage conflicts, increased environmental impacts and social perceptions, economic and political factors, regulatory constraints, license intricacies and lack of clear policy and management (Gentry et al., 2017; Matarazzo Suplicy, 2018). Consequently, the industry has reached saturation stage inshore, forcing aquaculture developments to move offshore. As the industry locates to highly hydrodynamic areas with better water quality conditions, it removes spatial constraints, potentially reducing ecological impacts while increasing production capacity (Gentry et al., 2017; Kapetsky et al., 2013; Lacoste et al., 2018). This paper defines 'offshore aquaculture' as.

'the establishment of aquaculture farms in exposed locations, in areas with a high energy environment and exposed to substantial oceanic conditions (large waves, storms and strong currents) located more than 1 km from the nearest coast and requiring reasonable infrastructure' (Mascorda-Cabre et al., 2021).

A continuous longline design is the most employed technique to grow mussels (e.g. *Mytilus edulis*), requiring minimum infrastructure while providing high crops (Avdelas et al., 2021; Scridel et al., 2020; STECF, 2018; STEFC, 2023). Although very attractive for the industry, the intensification of mussel farming in sheltered areas can have detrimental environmental impacts due to an increased amount of biodeposits (Mascorda-Cabre et al., 2021). In highly hydrodynamic areas

* Corresponding author at: University of Plymouth Marine Institute, 3rd Floor Marine Building, Drake Circus, Plymouth PL4 8AA, UK.
E-mail address: llucia.mascordacabre@plymouth.ac.uk (L. Mascorda-Cabre).

https://doi.org/10.1016/j.aquaculture.2024.740697
Received 16 March 2023; Received in revised form 16 February 2024; Accepted 20 February 2024
Available online 21 February 2024

where strong currents, waves and winds occur, longline farms are submerged 3 to 10 m. This technique has become a preferred method as it allows mussels to grow faster, have higher meat/shell ratios and produce higher yields (Kapetsky et al., 2013).

Contrary to inshore developments, high energy currents in offshore mussel farms are capable of dispersing biodeposits and significant volumes of organic loading with the potential to disperse them and reduce the farm's ecological effects (Lacoste et al., 2018; Lin et al., 2016). However, large farm developments may have an effect on water currents, causing blockage to the flow and dissipating energy, with the potential to alter environmental conditions (Plew et al., 2005, 2006; Zhong et al., 2022). This would affect the rate of biodeposit accumulation and potentially extending the footprint of a farm over larger areas (Giles et al., 2009; Lacoste et al., 2018), with a subsequent modification of pelagic and benthic communities and ecosystems (Mascorda-Cabre et al., 2023). Hence, there is a strong relationship between the hydrodynamic regime surrounding a mussel farm and the extent of its ecological and environmental effects (Lacoste et al., 2018; Lin et al., 2016).

Despite its potential benefits, it is still not fully understood how water flow changes due to the presence of a farm, how it can affect the hydrodynamic regime of the area (Lin et al., 2016) and, subsequently, its potential ecological impacts. This study aims to assess the effects that an offshore suspended longline mussel aquaculture farm located in Lyme Bay, UK, has on water circulation and the overall hydrodynamics of its surrounding environment to understand its potential footprint.

1.1. Study area: Lyme Bay

Situated in the Southwest of England, Lyme Bay is a large, open embayment stretching 65 km from east to west (Fig. 1), with a basic bathymetric profile showing a moderate slope from the intertidal zone to up to 50 m depth. Lyme Bay has a semi-diurnal tidal cycle (12 h, 12.42 h) (see later Fig. 5), with tidal amplitude ranges from 4.4 m to 1.9 m (springs and neaps respectively) at the west of the bay, to 3.4 m and 1.4 m (springs and neaps respectively) at the east. Tidal streams are bidirectional travelling east and westward parallel to the coast in a clockwise manner in concordance with the main English Channel tidal stream (Cefas, 2015) Lyme Bay currents are predominantly driven by a combination of regular and predictable tides as well as more dynamic wind and density effects. The eastwards tidal stream runs from two/three hours before high water (HW-2/3 h) until three/four hours after HW (HW + 3/4 h) at Exmouth, then it reverts to a westward flow (Cefas, 2015).

A previous study found peak tidal current velocities in the vicinity of the mussel farm to be 0.51 ms^{-1} westward and 0.36 ms^{-1} eastward with an estimate tidal excursion of about 7 km and 3.5 km during spring and neap tides respectively. Due to the effects of friction, flows near the seabed and in shallower near shore areas are likely to be slower. Even with the uniform bathymetry in Lyme Bay, significant water column mixing is likely to occur through friction and tidal action hence density, winds and waves play an important role in the oceanography and ecology of the Bay (Cefas, 2015; Mascorda-Cabre et al., 2023).

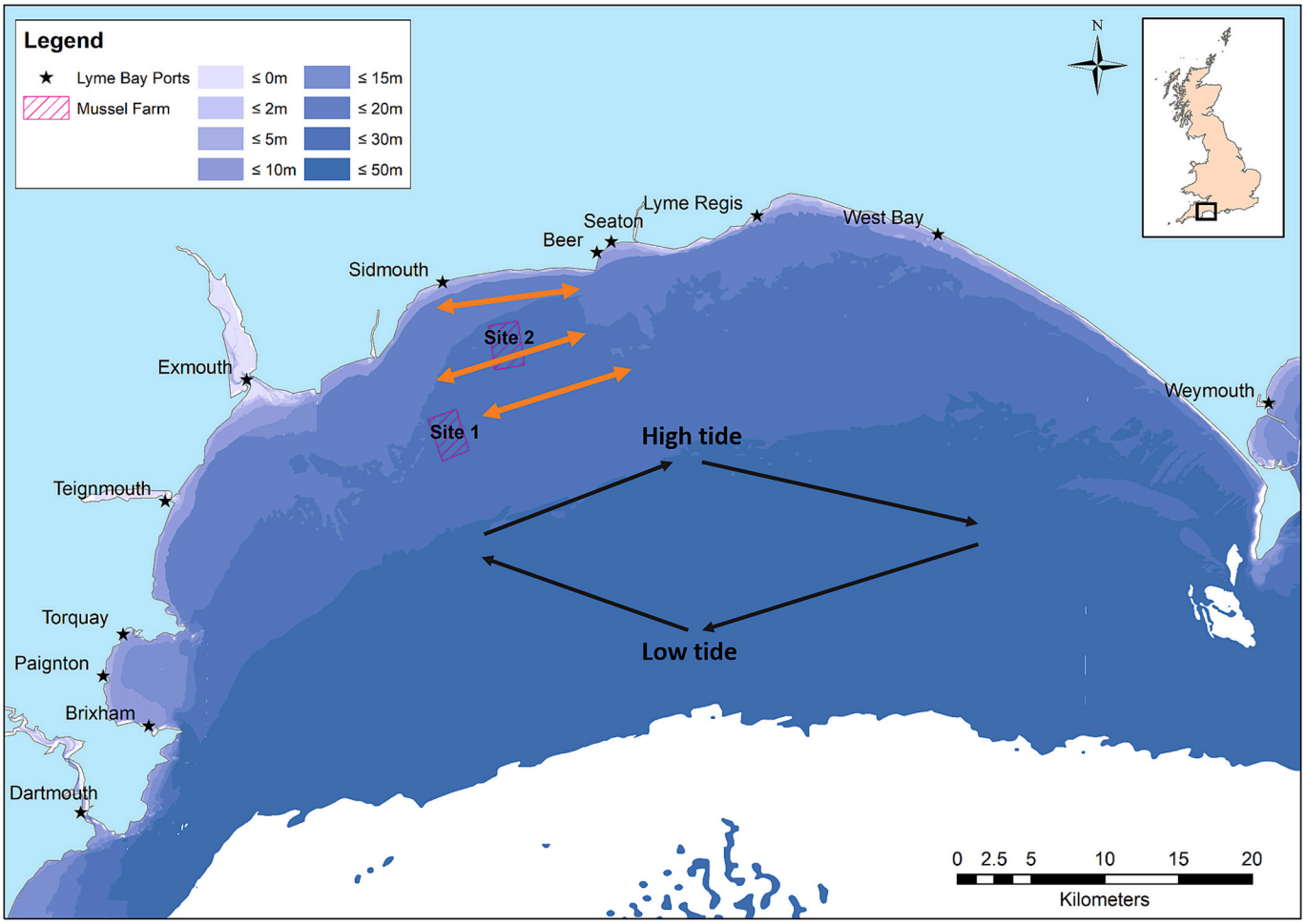

Fig. 1. Lyme Bay bathymetry map showing the main rivers and estuaries as well as position of the mussel farm. Black arrows indicate clockwise direction of tidal currents with eastward on the flood (HW -2/3 h to HW + 3/4 h - mean direction of 56°N) and westward on the ebb (LW + 3/4 h to LW-2/3 h - (mean direction of 242°N). Orange arrows indicate approx. Tidal stream direction and spring excursion within the farm's site (Cefas, 2015).

1.2. Influence of offshore mussel farms on water circulation

The presence of obstacles to water flow, including hard structures such as breakwaters or porous obstacles like kelp or seagrass beds, have a hydrodynamic impact, modifying flows at varying scales and magnitudes depending on the obstacle's size and nature (Chen et al., 2019; Hondolero and Edwards, 2017; Plew et al., 2006). As reviewed by Mascorda-Cabre et al. (2021), the establishment of a mussel farm in a highly hydrodynamic bay can potentially perturb the local water flow regime conditions (Fig. 2) by:

- *Attenuating currents and waves downstream of the farm*: as a physical obstacle to the flow, offshore mussel farms induce drag to the flow which results in a redistribution and reduction of the flow. The farm is likely to reduce current velocities within its boundaries, attenuating wave and current energy and, can increase water residence time and phytoplankton depletion which can have a knock on effect on water renewal and overall carrying capacity of the system (Lin et al., 2016; Plew et al., 2005, 2006; Zhong et al., 2022).
- *Accelerating currents beneath and above mussel ropes*: as longline mussel farms do not extend over the full water depth, reduced current velocities within the farm may cause a redistribution of the flow producing acceleration of currents above and beneath the mussel ropes (headlines are suspended 3–10 m below the sea surface), the latter being predominant. Beneath the ropes, acceleration may in turn generate greater bed friction and total drag (Plew et al., 2006; Zhong et al., 2022), transporting biodeposits and resuspended sediments further afield, impacting material transport and altering the overall farm's footprint (Mascorda-Cabre et al., 2021).
- *Altering current direction on the flanks of the farm*: redistribution of flow may also induce changes in vertical and horizontal circulation. Longline mussel farm dimensions are two to three orders of magnitude greater horizontally than vertically hence, horizontal effects would be greater, causing the flow to accelerate on the flanks of a mussel farm (Plew et al., 2005, 2006).
- *Increased susceptibility to shear-induced turbulence*: as mussel ropes generate drag-induced water flow velocity modifications, turbulence within the canopy may be generated as tidal streams pass through mussel covered ropes, potentially enhancing water column mixing (horizontally and vertically) and, disrupting water stratification (Plew et al., 2005, 2006).
- *Producing a wake downstream of the farm*: as upstream longlines divert water flow, producing lower within-farm velocities and acceleration around and beneath it, this may produce flow recirculation, determining the formation of a wake downstream of the farm (Plew et al., 2005, 2006; Zhong et al., 2022).

To investigate the role that the UK's first large-scale offshore longline mussel farm has on the above impacts, observational data were collected and analysed to test the hypothesis that the farm would generate: (i) current attenuation within the farm boundaries, (ii) current acceleration underneath, above and at the flanks of the farm, (ii) farm-induced shear changes and, (iii) sea surface (ss) current attenuation during high wave events.

In order to resolve these questions, investigations were performed using moored and vessel mounted Acoustic Doppler Current Profilers (M-ADCP and VM-ADCP) to: (a) establish the area's predominant tidal regime, wave directions and background currents (M-ADCPs); (b) study tidal constituents to establish farm-induced current velocity attenuation and acceleration beneath the ropes (M-ADCPs); (c) determine overall current velocity changes between downstream and upstream of the farm (M-ADCPs); (d) analyse current velocity changes near mussel headlines provided by transects parallel to the east and west flanks of the farm (VM-ADCP); (e) understand the potential of the farm to produce shear-induced turbulence changes by computing shear as a proxy measure of instability and turbulence changes (M-ADCPs) (Turner, 1973); (f) investigate sea surface current attenuation during storm events by comparing current velocity changes downstream and upstream of the farm (M-ADCPs) and; (g) assess velocity changes at different depths and at the flanks of the farm by comparing upstream and downstream transects along the east and west sides of the farm (VM-ADCP).

2. Methods

2.1. Study site: Offshore shellfish longline mussel farm

The focus of this study is the UK's first large scale offshore, suspended longline rope cultured mussel farm, operated by Offshore Shellfish Ltd. (OSL). The mussel farm is located in an exposed area between 3 and 10 km offshore in depths between 20 and 30 m relative to chart datum (Fig. 1). The farm deploys suspended longline ropes to cultivate the native blue mussel *Mytilus edulis*. This study is focused on Site 2, the most developed site of the farm.

Each 150 m long mussel headline is moored to the seabed with a pair of screw anchors. The headlines are suspended 3 m below the sea surface from a series of tubular buoys at regular intervals to keep the structure afloat. From the headline, a series of 'dropper' loop ropes extend a further 10 m down, upon which the mussels naturally attach (Fig. 3A). As far as possible, headlines are placed following the bathymetry of the area and parallel to each other at 50 m intervals (Fig. 3C). Headlines along the same bathymetry line are separated between each other by a 250 m gap (Fig. 3B). This arrangement ensures the dropper lines are suitably damped against wave action. At the time of this study, Site 2 had 128 stocked longlines from a total of 186 headlines. The Lyme Bay mussel farm was designed to withstand the highly hydrodynamic conditions of the area (Mascorda-Cabre et al., 2023).

Even though the farm is fairly sheltered from northerly winds, it is highly exposed to westerly and south-westerly winds and swells from the south, which are likely to be most effective in generating energetic wave action in the vicinity of the farm (Cefas, 2015).

2.2. Oceanographic mooring and vessel-mounted measurements

To resolve the attenuation of currents and waves and obtain continuous current velocity measurements, monitoring several tidal cycles, two 600 kHz WorkHorse Monitor RDI ADCPs were moored to a bedframe looking upwards (M-ADCP) on the east and west sides of the farm submerged to a mean depth of 25.7 m and 25.0 m respectively (stars Fig. 2). The ADCPs continuously sampled at 1 s intervals with a bin size of 0.75 m and sampled 20-min wave burst every hour. The height of the first good bin was at 1.85 m above the seabed. The west M-ADCP location was chosen to be where most of the ropes were layered (higher headline density) and, the east M-ADCP was located east of the farm, on the same depth contour as the west M-ADCP. The area's predominant tidal direction is west-east hence M-ADCPs were on the upstream or downstream at each phase of the tide (as verified by study results). On each phase of the tide, the upstream M-ADCP served as a control point to establish the unperturbed flow (where no ropes or flow obstructions were present), whereas the downstream M-ADCP was expected to resolve any impacts of the farm. To resolve the spring-neap cycle and capture the impact of any energetic events associated with either local or remote storm forcing, M-ADCPs were deployed on June 29, 2021, and recovered on August 11, 2021, producing a total of 45 days of data.

The M-ADCP survey was complimented by two vessel mounted (VM-ADCP) surveys using a 600 kHz WorkHorse Monitor RDI ADCP mounted to a vessel looking downwards. With the aim of resolving changes in flow within the farm, the ADCPs were set to sample at 3 s intervals with a bin size of 1 m and the depth of the first good bin at 1.95 m below the sea surface.

The first survey was performed along the east and west limits of the farm (purple and green arrow transects, Fig. 2) during an entire tidal cycle on a spring tide (13 h on 12th July 2021) to determine differences

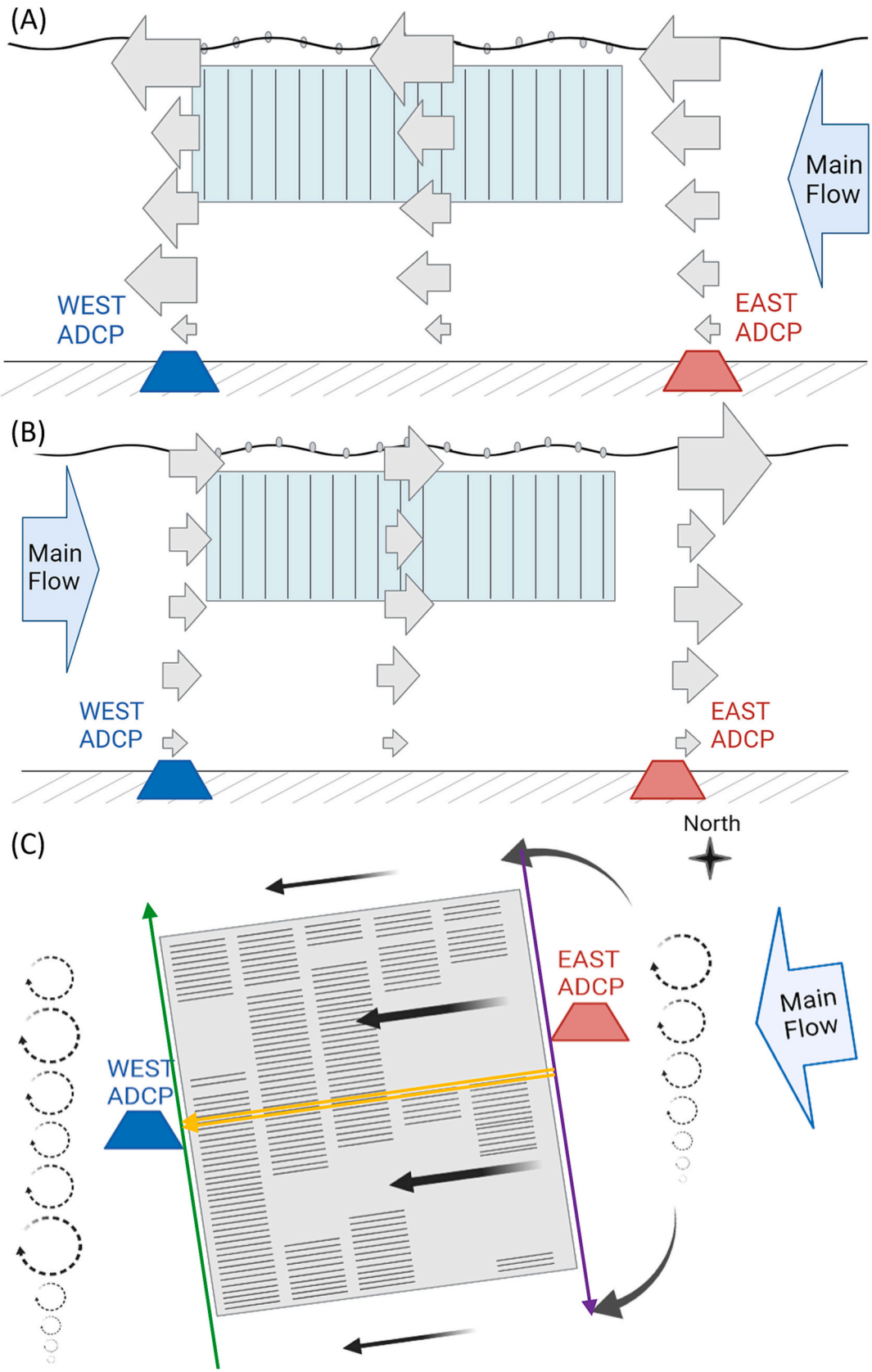

Fig. 2. Offshore longline mussel farm ADCP surveys displaying the position of two M-ADCPs (West-blue and East-red) and VM-ADCP surveys (yellow, purple and, green arrows) in relation to the farm under study as well as mussel headline density at the time of the survey. The diagram displays potential farm-induced flow changes from an elevation (A, B) and plan (C) views indicating the various hydrodynamic processes under study: within-farm water flow and current attenuation (A, B), surface acceleration (A, B, C), flank acceleration (C), accelerating undercurrent (A, B) and mixing layer (C) (not to scale). (For interpretation of the references to colour in this figure legend, the reader is referred to the web version of this article.)

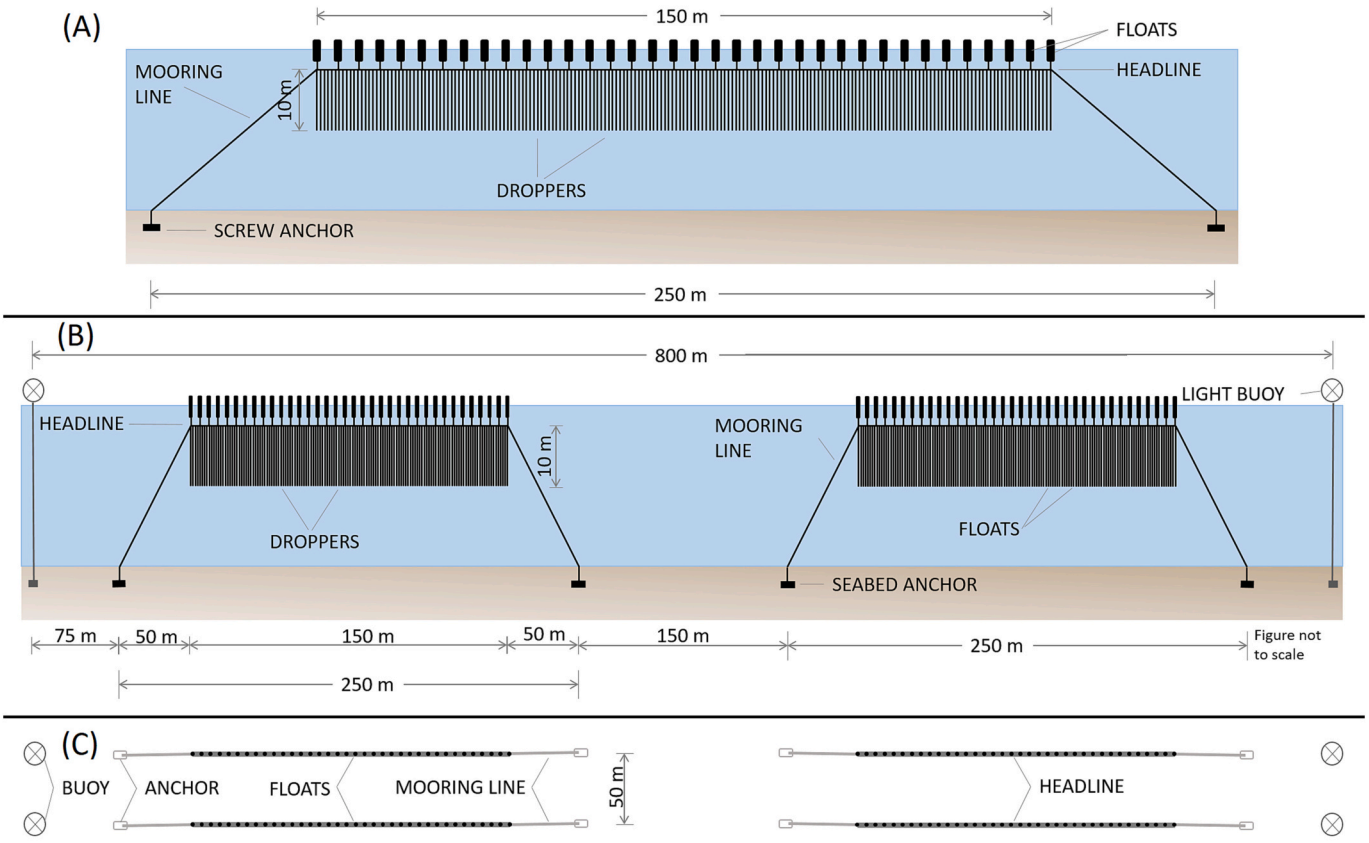

Fig. 3. Design of Offshore Shellfish Ltd. farm. (A) Single headline profile; (B) farm profile; and (C) plan of the farm.

in current velocities between the upstream and downstream of the farm as well as changes in current direction on the flanks of the farm. Boat transects were performed as close to the headlines as possible but due to the risk of dropper and headline tangling, a safe distance was kept.

To capture the highly localised impact of the farm on currents between and beneath the mussel ropes, a second VM-ADCP survey was performed during a very calm summer day on August 2, 2021, at ebb, on a neap tide (yellow arrow transect, Fig. 2). Two transects along the entire length of the farm, parallel to two headlines were performed to obtain more in-depth information on the effect of the headlines on the flow. The lines were chosen to be in the middle of the farm to focus on the area with highest mussel and headline density (near both moored M-ADCPs).

2.3. Wind data

Wind data for the duration of the M-ADCP survey were obtained from the Copernicus Marine Data. Global Ocean Hourly Sea Surface Wind and Stress from Scatterometer and Model (WIND_GLO_PHY_L4_NRT_012_004) was used. The spatial resolution of the satellite data was 0.125°x0.125° (EU Copernicus Marine Service, 2022).

2.4. Data processing, treatment and, analysis

Prior to conducting the analysis, current data were output as three components (u – positive eastward, v – positive northward and, w – vertical). According to the embayment orientation and the shore face configuration (facing South with contour lines parallel to the shoreline) and, given the orientation of the farm (Fig. 1), it was necessary to rotate the coordinate system to extract current components parallel and perpendicular to the longlines to obtain upstream and downstream velocities. All data series were interpolated for both time and depth, cleaned, and smoothed with 9 points median and 9 point running average filter respectively, to obtain comparable data sets.

2.4.1. Tidal analysis

To isolate the tidal contribution to the observed currents and, resolve the residual current from the recorded, classical tidal harmonic analysis was performed using T_TIDE tool with MatLab© (Pawlowicz et al., 2002). Predicted tidal velocities were estimated using those tidal constituents with a signal-to-noise ratio > 2. The predicted total currents for the measured period were constructed from the contributions of 35 tidal constituents (Supplementary material Table I and Table II), including major semidiurnal tidal constituents M_2, S_2, N_2, Mu_2, L_2; major diurnal constituents K_1, O_1, J_1, Q_1; long-period constituents MM and MSF and; higher harmonics M_4, M_6 and S_4 for shallow water constituents (Lopes and Tenreiro Machado, 2017; Simon and Page, 2017). This analysis was used to identify the deterministic barotropic or phase-locked baroclinic currents in the M-ADCP data that could be altered by the presence of the farm. Following this, depths for which the predicted ellipse properties showed potential alterations due to the farm's presence were isolated for further study. M_2 was the major tidal constituent used for further analysis.

2.4.2. Wave and wind analysis

To locate periods of particular wave height and storms causing increased water current velocities, the long-time wave series was analysed in detail for wave height (Hs), peak wave period (Tp - period associated with largest peak in power spectrum) and peak wave direction ($°Dp$ - peak direction at the peak period) for both M-ADCPs. Wave roses were plotted using MatLab© (Pereira, 2023). Fully directional wave spectra were estimated from 20-min M-ADCP bursts using RDI

WavesMon software.

2.4.3. Upstream and downstream current determination of M- ADCP data

Depending on the flow's direction (westward - negative *u* or eastward - positive *u* velocities), west and east M-ADCP data were separated as downstream or upstream. For instance, to measure the effect of the farm on westward currents, negative *u* velocities for both east and west M-ADCP were plotted as upstream and downstream respectively.

Due to the orientation of the farm (Fig. 2) and the predominant tidal (orientation of the tidal ellipses (Fig. 4)) and current regime, M-ADCP data was rotated 30° previous to any analysis. This allowed us to find along- and through-farm current components rather than east-west *u* velocities and north-south *v* velocities respectively, obtained by the M-ADCPs. Along-farm velocity currents had a positive and negative component for eastward and westward currents respectively. Through-farm velocity currents also had a positive and negative component for northward and southward currents respectively. Thus, for the comparison between upstream and downstream currents, along- and through-farm velocities were used.

To assess sea surface velocity changes during higher-than-average wave events (>1 m) produced by south-westerly storms, only through-farm velocities where use.

2.4.3.1. Residual circulation. To further assess upstream and

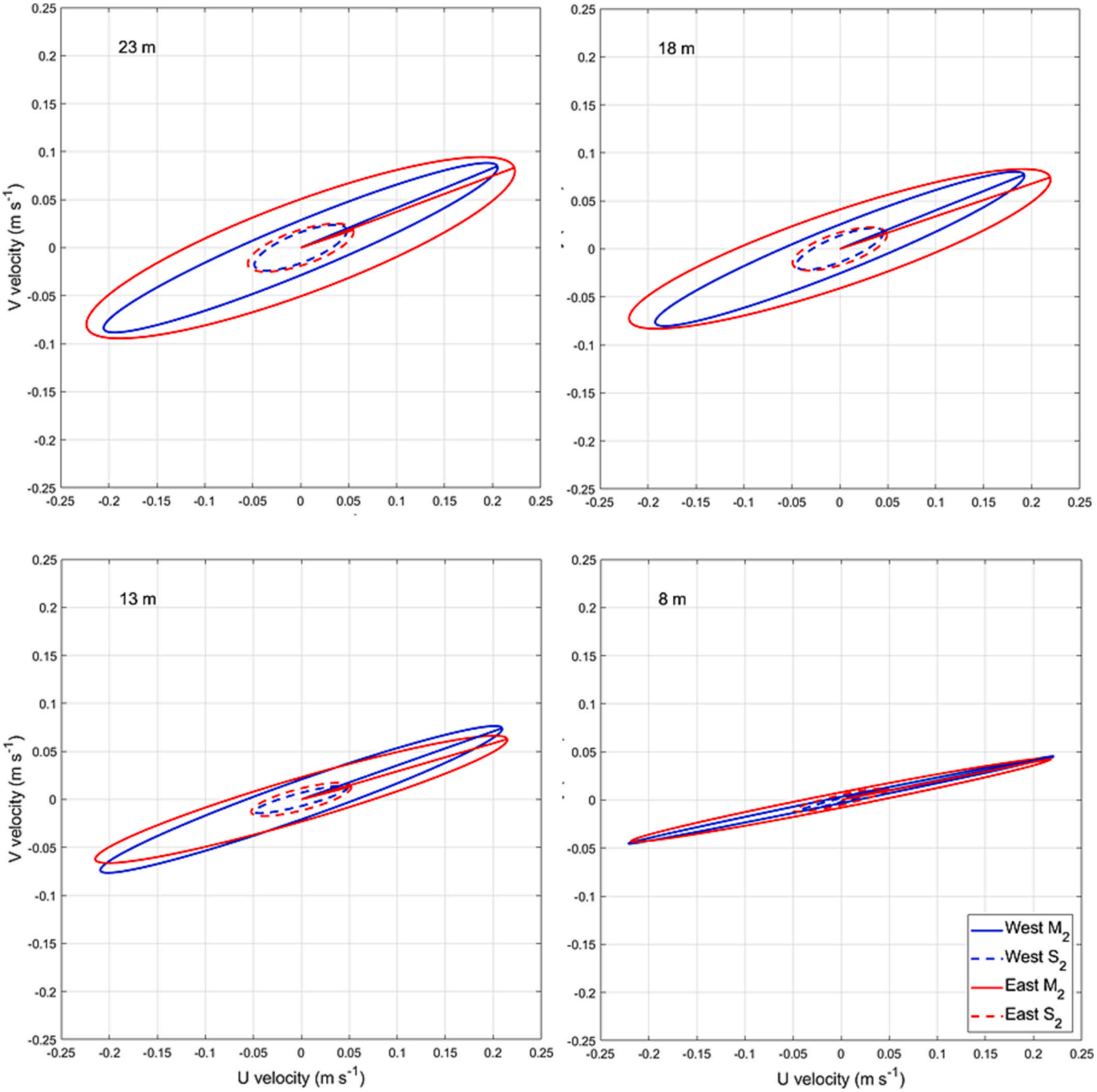

Fig. 4. Tidal ellipses for M_2 (solid line) and S_2 (dashed line) plotted at four different depths: 23 m – top-of-droppers (3 m below ss, where the headlines are suspended); 18 m – mid-droppers (8 m below ss); 13 m – bottom-of-droppers (14 m below ss) and; 8 m – below-droppers (27 m below ss) from both the west (blue) and east (red) M-ADCPs. (For interpretation of the references to colour in this figure legend, the reader is referred to the web version of this article.)

downstream signal effects along the water column, the tidal velocity component estimated by T-TIDE was extracted from measured M-ADCP currents to obtain residual currents not affected by the tide.

2.4.4. Shear instability analysis

To assess the potential of farm-induced turbulence changes generated by the overturning of stratification, vertical current shear (Turner, 1973) was calculated as $S^2 = ((\partial u / \partial z)^2 + (\partial v / \partial z)^2)$, where u and v are the eastward and northward velocity components respectively and, their gradient is computed over a depth range. Shear was computed over the 0.75 m vertical intervals corresponding to the M-ADCP bin sizes.

3. Results and discussion

3.1. Predominant local conditions: Tidal regime and waves

Prevailing flow conditions around the mussel farm were studied through the analysis of tidal and wave data time series.

3.1.1. Tidal regime

Tidal harmonic analysis was performed to compare changes in tidal motions between both M-ADCPs and, identify the orientation of the semi-major axis of the tidal ellipse for each constituent. Results showed an overall decrease in tidal speed and an increase in the ellipticity with depth, in line with seabed friction. Predominant tidal currents were orientated east-west (Fig. 4) demonstrating that both M-ADCPs were located in the appropriate position in regard to the farm and the predominant water flow (Fig. 2). This allowed to effectively assess the interaction of the farm on the flow.

As the two dominant tidal constituents, tidal ellipses were computed for the M_2 and S_2 and plotted at different depths to understand changes in tidal currents throughout the water column (Supplementary material Table III and Table IV). Key depths were identified as areas where the effects of the farm on the currents were predicted. These water depths relative to the seabed were used throughout this study to characterise the effects of the farm: 23 m – top-of-droppers (3 m below sea surface, where the headlines are suspended); 18 m – mid-droppers (8 m below ss); 13 m – bottom-of-droppers (14 m below ss) and; 8 m – below-droppers (27 m below ss).

When assessing the long-term time series, peak velocities during spring tides were 0.6 ms^{-1} with maximum velocities occurring at the ebbing tide on a westward direction. The maximum M_2 mean u velocity was found above the farm (sea surface – 0.24 ms^{-1}) in the east M-ADCP and beneath the farm (19 m below ss – 0.23 ms^{-1}) in the west M-ADCP; the minimum M_2 mean u velocity was found closest to the seabed in both M-ADCPs (east – 0.17 ms^{-1} and west −0.18 ms^{-1}). M_2 mean v velocity was consistently higher in the east M-ADCP than the west M-ADCP with maximum near surface values of 0.24 ms^{-1} and 0.13 ms^{-1} respectively. Minimum values were found near sea bottom with the lower values in the west M-ADCP compared to the east M-ADCP (0.05 ms^{-1} and 0.17 ms^{-1} respectively). At both M-ADCPs, there was a maximum difference of 0.04 ms^{-1} v velocity between the top-of-droppers (23 m) and below-droppers (8 m) ellipses. Throughout all depths, tidal velocities on the west M-ADCP were slower than on the east M-ADCP showing up to

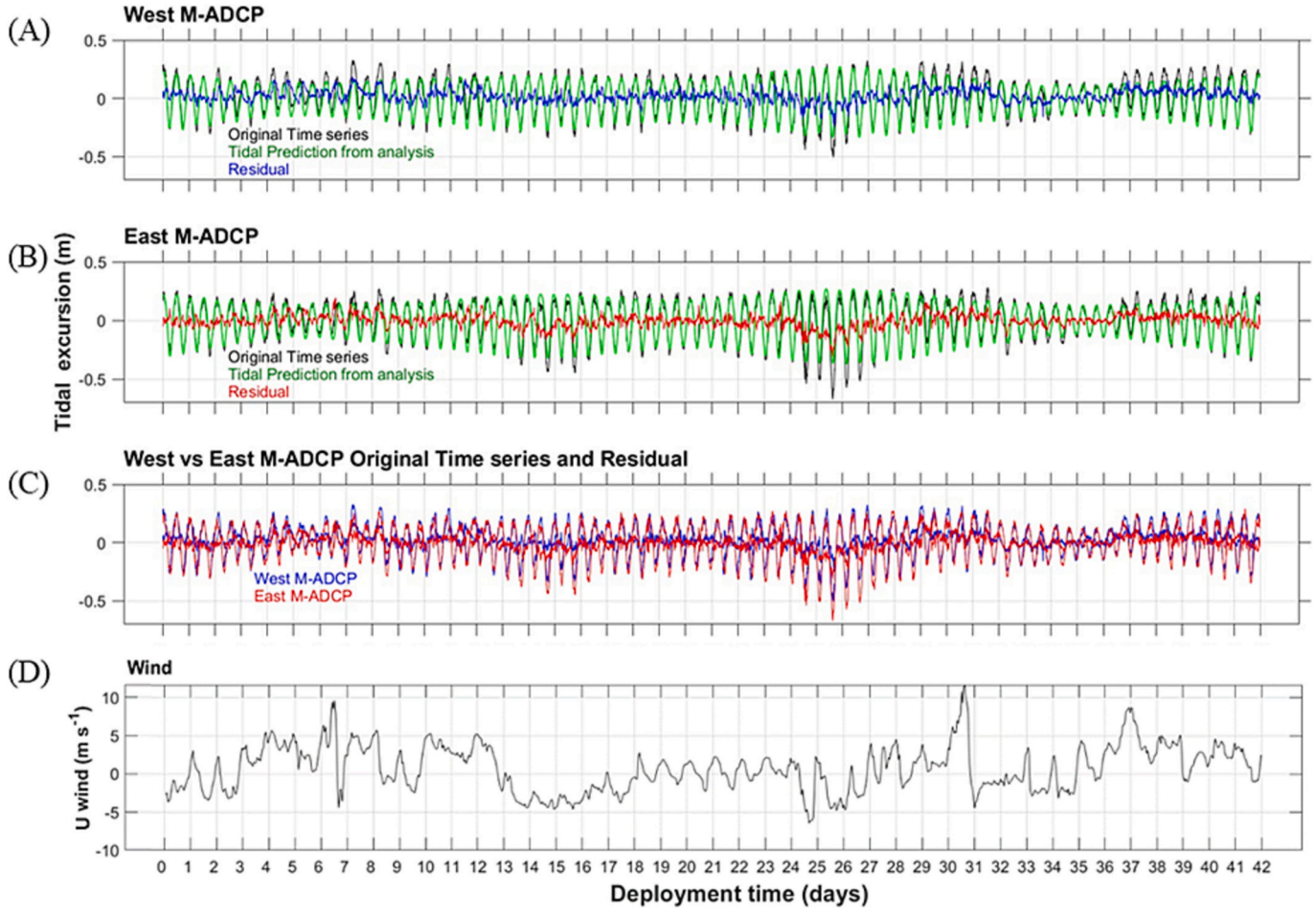

Fig. 5. Tidal excursion time series analysis for both M-ADCPs showing original tide time series (A and B - black), predicted tidal excursion (A and B - green) and the difference between original and predicted (A – blue, B – red) for both (C) west (blue) and east (red) M-ADCPs. North wind velocity (D) shows correlation with the residual currents. (For interpretation of the references to colour in this figure legend, the reader is referred to the web version of this article.)

0.027 ms^{-1} *u* velocity and 0.003 ms^{-1} *v* velocity differences. While west M-ADCP top-of-droppers and mid-dropper's ellipses had lower *v* velocities, ellipses under the farm at the bottom-of-droppers and below-droppers (13 m and 8 m respectively) showed stronger *v* velocities and weaker *u* velocities compared to east M-ADCP, demonstrating tidal velocity changes induced by the farm.

Tidal excursions (distance travelled by tidal flow between slack low-water and high-water tide) extracted by T-TIDE (Fig. 5) were plotted for both west (A) and east (B) M-ADCP at 20 m depth showing time-series of original tide (A and B – black, Fig. 5), predicted tidal excursion (A and B – green, Fig. 5) and the difference between original and predicted as the residual tide (A - blue, B – red, Fig. 5). The residual and original tide (Fig. 5C) was plotted for both west (blue) and east (red) M-ADCPs. The original tidal excursion (A and B - black, Fig. 5) was extracted from measured M-ADCP currents to obtain the residual tide to analyse farm effects on non-tidal currents. The original and residual plot (Fig. 5C) showed overall weaker east M-ADCP tidal and non-tidal currents especially when eastward currents occurred (downstream of the farm), while when westward currents occurred, the west M-ADCP (downstream of the farm) showed weaker tidal and non-tidal currents, demonstrating that the east and west M-ADCPs effectively alternate between being upstream and downstream of the farm.

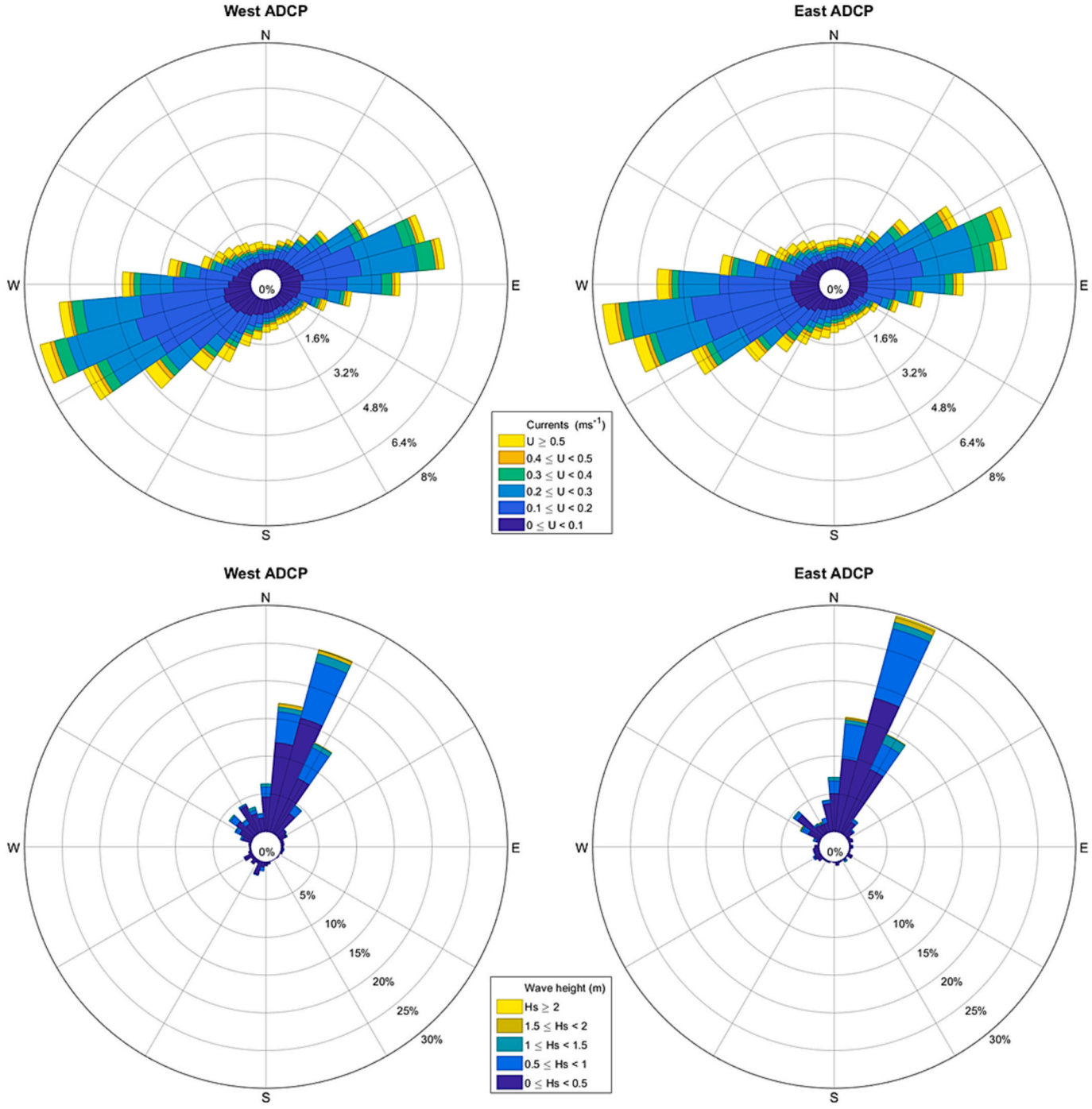

Fig. 6. Current (top) and wave (bottom) rose depicting predominant current magnitude and direction (top) and wave height and direction (bottom) for both west and east M-ADCPs. (For interpretation of the references to colour in this figure legend, the reader is referred to the web version of this article.)

3.1.2. Wave events

For both M-ADCPs, wave regime was characterised by more likely sea states from the southwest (Fig. 6). Events with continuous wave height of >1 m for >6 h (half a tidal cycle) were highlighted. Higher than average wave heights coupled with extreme wind conditions (winds of up to 10 ms^{-1}) were identified to be part of one summer storm event registered 29th to 30th July (Storm Evert) and two smaller summer storm events registered on 5th July and 4th August (shaded bands, Fig. 7).

Over the course of the survey, both M-ADCPs recorded a tidal elevation range that reached 1 m (Fig. 6 - top) with maximum recorded wave heights (H_s) of 2.06 m and 2.09 m for the west and east M-ADCPs respectively (Fig.6- top and Fig.7). The west M-ADCPs registered an averaged significant wave height (H_s) of 0.38 m (± 0.33 m) with a peak wave period (T_p) of 5.45 while east M-APDC had an averaged significant wave height of 0.42 m (± 0.35 m) and a T_p of 5.4. Both M-ADCPs recorded similar values of H_s, with a variation of up to 0.1 m greater for the east M-ADCP, even though east M-ADCP was at a greater depth than west M-ADCP.

3.2. Farm-induced flow changes

To assess farm-induced flow changes, tidal and residual M-ADCP current velocities depth-profiles were studied to determine aquaculture-induced velocity changes such as water flow blockage, acceleration of currents beneath the farm (downwelling), increased vorticity and vertical circulations and, the potential increase in shear-induced turbulence within the farm.

The study of VM-ADCP current velocities were performed by depth-averaged analysis at particular depths to aid data description and representation. Depths were chosen to represent key areas throughout the farm's water column: the top-of-droppers (2–4 m); mid-droppers (7–9 m); bottom-of-droppers (12–14 m); below-droppers (19–21 m) and; the seabed (23–24 m).

3.2.1. Within-farm current attenuation and acceleration beneath the ropes

To identify whether current velocities were altered by the farm's physical boundaries (3–13 m below ss), producing velocity attenuation between the ropes but an acceleration beneath as water becomes squeezed under the farm, upstream and downstream currents were compared. The term 'within-farm' is used, from this point onwards, to describe the effects of the farm's droppers (physical farm's footprint) even if measurements were not physically taken from within the farm headlines.

3.2.1.1. Comparison of downstream and upstream currents. To assess whether observed tidal and residual current changes occurred along the water column and, to determine differences between the west and east M-ADCPs to investigate the effects of the farm on downstream currents, upstream and downstream (blue and red respectively) currents were extracted and compared as those westward (negative upstream and downstream velocities) or eastward (positive upstream and downstream velocities) (Fig. 8). Differences between upstream and downstream currents were also calculated (black lines, Fig. 8) showing the overall increase and decrease of flow speed along the water column.

Depth profiles of upstream and downstream along-farm currents showed within-farm current attenuation by the mussel ropes, with a clear increase in horizontal velocity beneath the ropes as water is compressed within the farm (Fig. 8). This signal was strongest with westward flows as per the area's predominant current (Fig. 6 - top), where mean tidal currents within the farm droppers' depths decreased by 28% from −0.105 ms^{-1} (upstream) to −0.075 ms^{-1} (downstream) and, under the mussel ropes velocity increased by 7% from −0.110 ms^{-1} (upstream) to −0.118 ms^{-1} (downstream). Near-seabed velocities increased by 11% (from −0.099 ms^{-1} to −0.110 ms^{-1}) while sea surface velocities decreased by 54% (from −0.087 ms^{-1} to −0.041 ms^{-1}). Eastward flows showed a similar pattern with lower impact where within the farm droppers' depths mean tidal currents decreased by 2% from 0.098 ms^{-1} (upstream) to 0.096 ms^{-1} (downstream) and, under

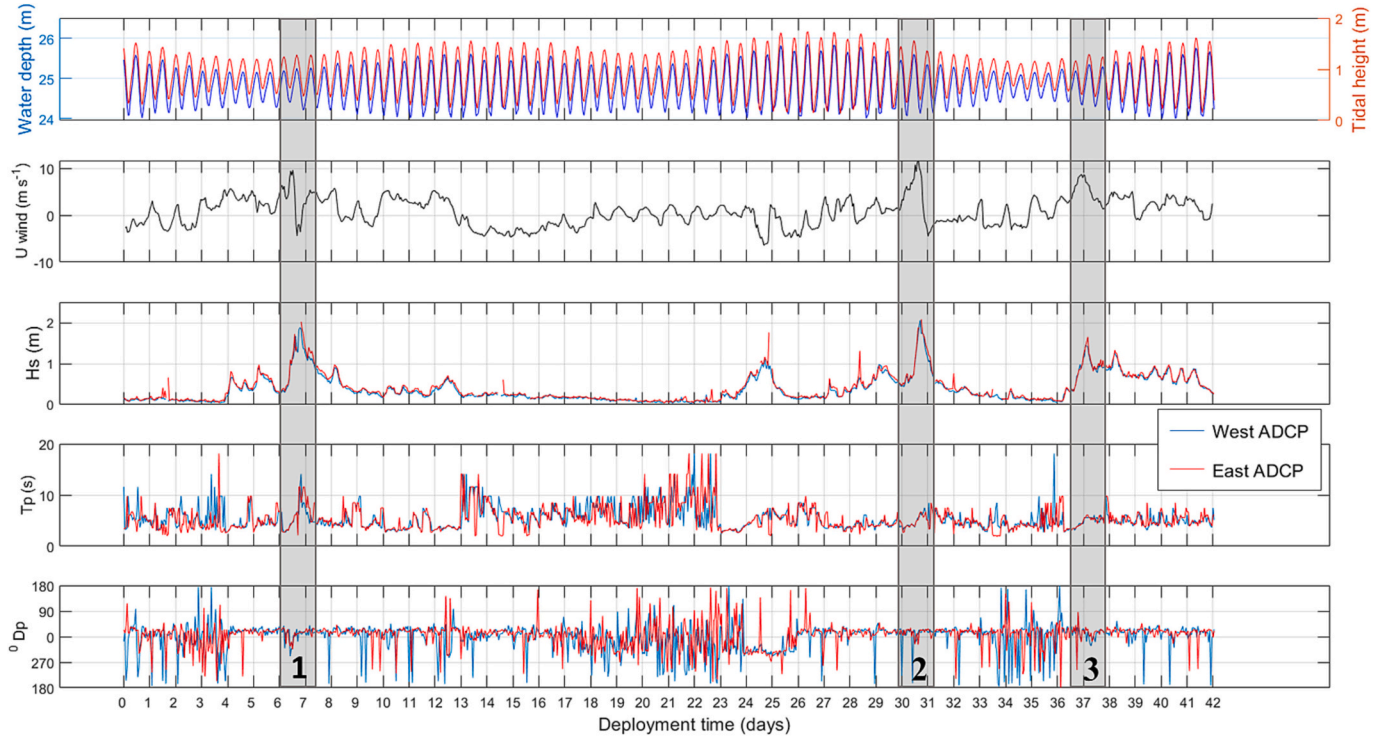

Fig. 7. Tidal height, wind velocity, significant wave height (*Hs*), peak wave period (*Tp*) and peak wave direction (°*Dp*, north at 0° and east at 90°) time series for both M-ADCPs (blue corresponds to west and red corresponds to east M-ADCP). Shaded bands show three summer storm events with wave heights of >2 m. (For interpretation of the references to colour in this figure legend, the reader is referred to the web version of this article.)

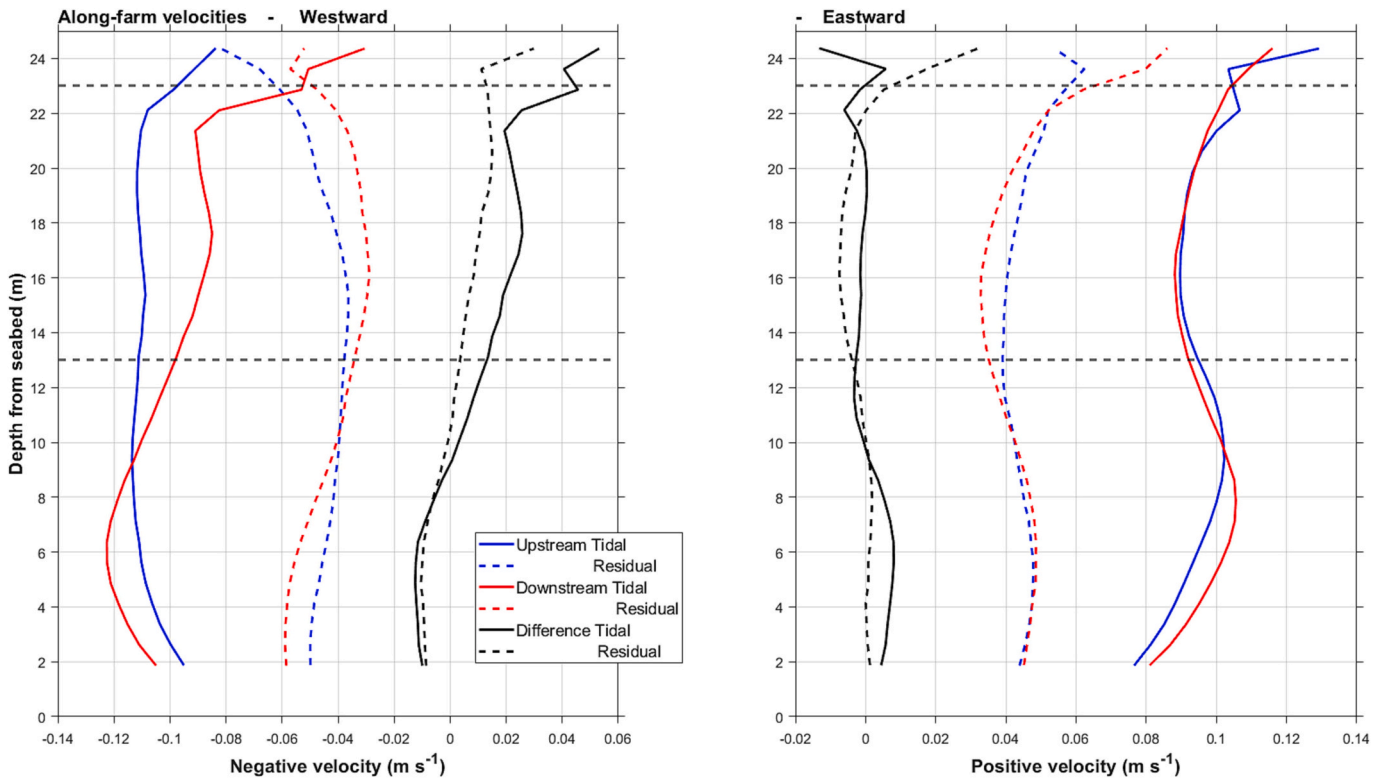

Fig. 8. Depth profiles of along-farm upstream and downstream tidal and residual current velocities of two M-ADCPs over farm boundaries (horizontal grey dashed lines). Black lines show velocity differences between upstream and downstream currents.

the mussel ropes velocity increased by 5% from 0.095 ms^{-1} (upstream) to 0.1 ms^{-1} (downstream). Here, near-seabed velocities increased by 7% (from −0.086 ms^{-1} to −0. 081 ms^{-1}) while sea surface velocities decreased by 3% (from −0.113 ms^{-1} to −0.116 ms^{-1}). This demonstrates water flow reduction through ocean sprawl and filter feeding mussels, with a consequent flow increase beneath, capable of dispersing and diluting mussel biodeposits. Currents decreased near the bottom due to seabed friction as expected.

Under offshore conditions, in deep waters, the largest velocity amplitude usually takes place at the seawater surface; however, this was only true during eastward tidal currents. This could be because wave propagation is larger on this direction (Fig. 6 - bottom). In westward currents, sea surface velocities were consistently lowest, with minimum ss velocities of −0.084 ms^{-1} (upstream) and − 0.031 ms^{-1} (downstream) compared to near-seabed velocities of −0.095 ms^{-1} (upstream) and − 0.115 ms^{-1} (downstream). This increase in near-seabed velocities of 21% between up and downstream can further enhanced dispersion of mussel biodeposits and it could have an impact in seabed sediment resuspension and dispersion (Mascorda-Cabre et al., 2021; Plew et al., 2006). There was a 171% increase in near-seabed velocity compared to sea surface velocities downstream of the farm (ss: −0.041 ms^{-1}; near-seabed: −0.110 ms^{-1}), further demonstrating the impacts of the farm on the flow.

Although farm surface currents increased with depth (0–3 m), from the sea surface to 3 m below ss (where the farm headlines are) from −0.031 ms^{-1} at ss to −0.091 ms^{-1} above the mussel headlines (increase of 66%), on the westward flows, ss velocities decreased from −0.084 ms^{-1} upstream to −0.031 ms^{-1} downstream (decrease of 63%).

These observations are in agreement with other longline mussel farm studies showing current reductions of up to 90% and farm flow decrease between mussel droppers of 25–30% and up to 63% (Lin et al., 2016; Plew et al., 2005, 2006).

To further assess the farm's interaction with the flow, residual currents were generated by removing the effect of the tide from original currents (dashed lines, Fig. 8). Results showed higher velocities at the surface and upstream of the farm (0.023 ms^{-1} difference) with decreasing along-farm velocities with depth. There is a clear decrease in within-farm residual currents due to mussel dropper's drag, with a consequent increase in along-farm velocities directly under the mussel droppers, further supporting the hypothesis that the mussel farm has an impact on the entire water column and downstream currents, reducing the effect of seabed friction.

3.2.1.2. Sea surface northward current attenuation during high wave events. Currents recorded by both M-ADCPs during three events recording continuous wave heights of >1 m for more than half a tidal cycle were used to assess aquaculture-induced sea surface current attenuation (Fig. 6 and Fig. 7). These events were used to determine sea surface flow attenuation during periods of atypical weather conditions where waves were northward on a predominantly westward current. Due to the northward direction of the waves, in this instance, the west M-ADCP was treated as upstream while the east M-ADCP was assessed as downstream. It was expected that through-farm positive velocities would be stronger on the west M-ADCP (upstream).

Depth profiles of through-farm upstream and downstream (blue and red respectively, Fig. 9) currents during an event with >2 m northward waves, showed how downstream velocities were significantly decreased. This result further supports those found when comparing the along-farm current attenuation by the farm. This signal was particularly strong when analysing through-farm positive velocities, where surface currents (waves) were reduced by 72% from 0.228 ms^{-1} (upstream) to 0.064 ms^{-1} (downstream). Through-farm negative velocities were reduced by 16% from −0.062 ms^{-1} (upstream) to −0.052 ms^{-1} (downstream). Differences between upstream and downstream currents were also calculated (black lines, Fig. 9) showing the overall increase and decrease of flow speed throughout the entire water column.

3.2.1.3. Mussel headlines-induced velocity changes. Two VM-ADCP

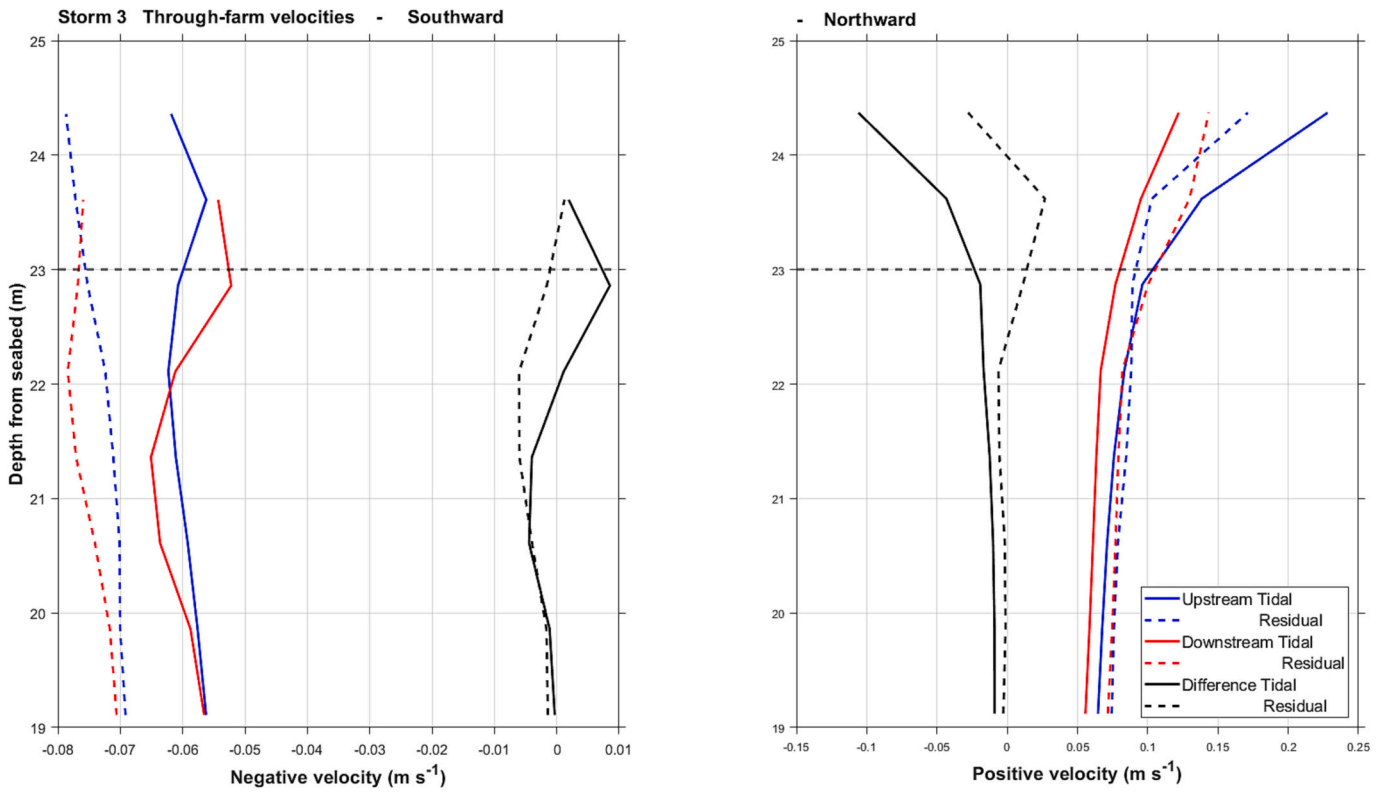

Fig. 9. Depth profiles of through-farm upstream and downstream tidal and residual current velocity from two M-ADCP over upper farm boundary (horizontal dashed line). Black lines show velocity differences between upstream and downstream currents. Flow arrow describes the direction of the flow.

transects were performed to further identify farm-induced velocity changes throughout the entire water column and throughout the entire length of the farm, complementing the M-ADCP study results.

Results from the VM-ADCP transects displayed changes in current speed and direction caused by the headlines (Fig. 10). The survey was performed during ebb tide when local currents were predominantly westwards. Five sets of farm headlines are displayed in Fig. 10 (blue rectangles) to aid analysis of result. However, headlines and, in particular droppers, are not static and move with the flow; therefore, changes in flow velocities were not expected to perfectly fit the location of the headlines and droppers as represented in the graph.

The greatest velocities were found above the headlines, on the sea surface (Fig. 10) and beneath the farm, supporting previous results showing an increase in sea surface velocities above the headlines (0–3 m) and the hypothesis that suspended farms accelerate velocities above and beneath the farm's physical footprint. In the middle of the transect, at 1 km from the beginning, mean u velocities at depths 2–4 m peaked at -0.30 ms^{-1} compared to -0.22 ms^{-1} 0.3 km earlier and $-$ 0.20 ms^{-1} 0.3 km later in the transect. The lowest velocity recorded at that depth was -0.06 ms^{-1}, showing an increase of 80% mean u velocities in 0.5 km within the same transect. Velocities decreased towards the seabed by 0.1 ms^{-1} falling to -0.24 m s^{-1} at the centre of the transect compared to -0.12 ms^{-1} and -0.11 ms^{-1} 0.3 km before and after respectively. Depth bins underneath the farm (19–21 m) exhibited consistently higher currents than the bins above (7–9 m and 12–14 m), indicating that rather than the attenuation of currents with depth towards the bed by friction, currents increased under the farm, suggesting acceleration by convergence and downwelling. This effect was observed on the first 1.2 km of transect, which corresponded to the east side of the farm, the most developed part.

Velocity vectors showed an overall increase of sea surface velocities, followed by a decrease of within-farm u velocities. This is followed by an acceleration beneath the ropes to then decrease due to seabed friction. As headlines are separated by a 250 m gap, this empty space appeared to have faster velocities (Fig. 10), especially in the centre of the farm, as shown by depth-average velocities. This demonstrated big local flow perturbation by the farm as, given the short distance of the transect (2 km), even if flow isn't laminar, no considerable changes in flow such as those recorded, would be expected. Due to an overall inequality between the amounts of developed headlines on the eastern part of the farm compared to the western side (insert, Fig. 10), flow distortion was more pronounced on the first half of the transect.

Whereas most of the headlines were found in the west side of the farm (first three columns from the west), the eastern part (last two columns) had less than half the developed headlines reducing the drag and within-farm velocity changes.

This study allowed us to obtain higher level of understanding of within-farm velocity changes and how these were dependent on both the state of the tide at the time of study and, the number of developed ropes, which would provide more or less drag depending on the size and abundance of mussels. In addition, this study allowed us to observe that the overall farm-induced velocity changes were a combination of slower u velocities, a change in flow direction coupled with in-between-headline flow acceleration.

3.2.1.4. Farm-induced turbulence changes (shear). To explain within-farm velocity attenuation and acceleration beneath the ropes, shear (S^2) was calculated, as a proxy measure. Shear was used to evaluate changes in water flow instability and turbulence, as it describes the magnitude at which layers in a stratified fluid flow differently from one another. In a free-flowing fluid, bottom friction causes a logarithmic velocity profile where velocities decrease as fluid gets closer to the bottom (Plew et al., 2006) hence, shear should increase as depth increases. In the absence of a farm, velocities should decrease logarithmically from the sea surface to the seabed and shear should increase towards the seabed. However, due to the introduction of drag forces by the farm, this pattern was altered (Fig. 11). For instance, during

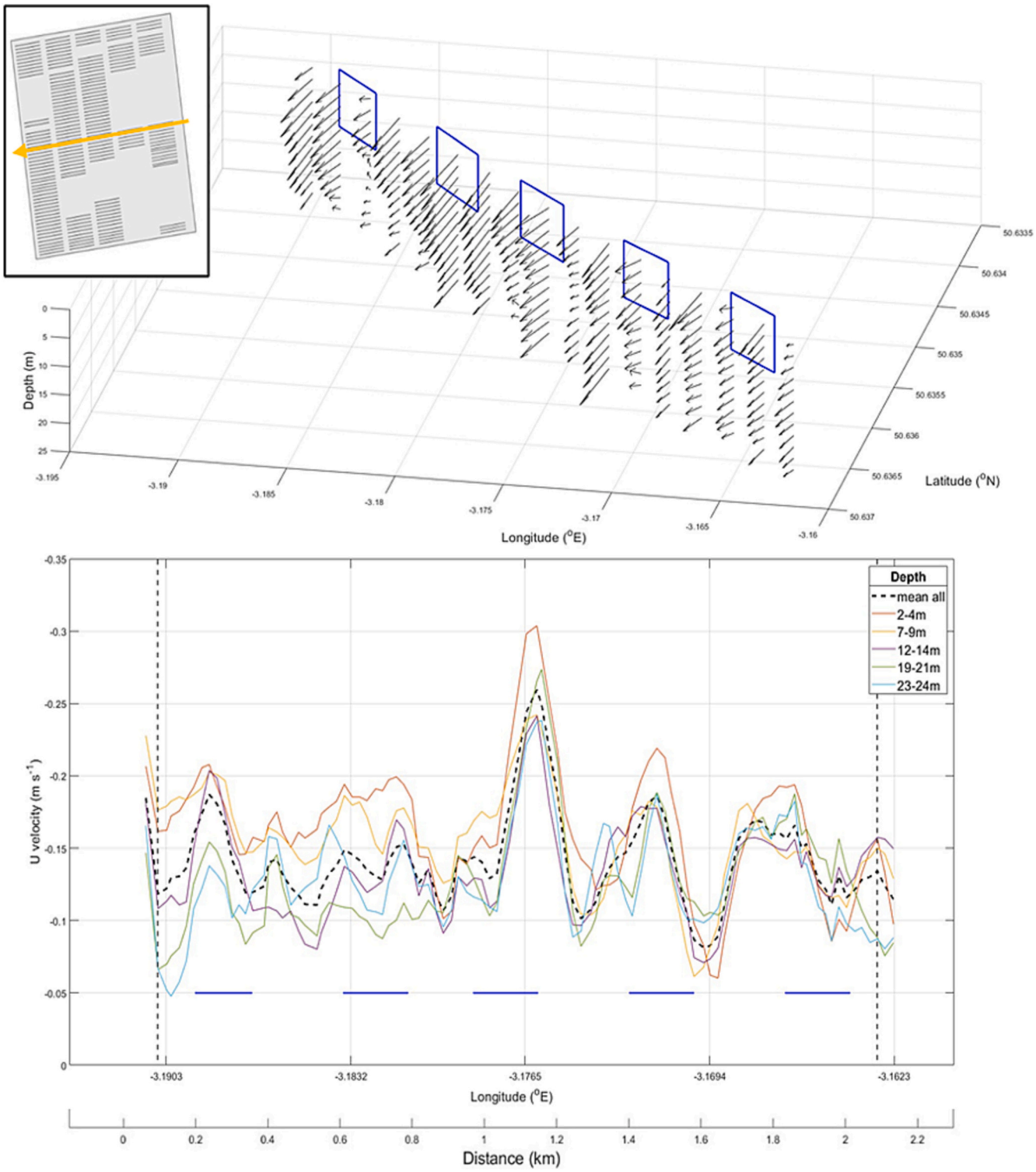

Fig. 10. *U* velocities found in a VM-ADCP survey performing transects parallel to the farm's headlines showing (top) velocity vectors and (bottom) *u* velocity depth profiles. Depths have been chosen to represent: the top-of-droppers (2–4 m); mid-droppers (7–9 m); bottom-of-droppers (12–14 m); below-droppers (19–21 m) and; the seabed (23–24 m). Overall mean depth *u* velocity is represented by a black dashed line. Farm boundaries (grey dashed lines) and transect headlines (blue lines/rectangles) are shown. Blue rectangles represent the extent of mussel headlines and droppers. Insert diagram shows the transect position in relation to the farm. Note: For better vector visualisation, east of the farm (start of the transect) was placed on the right of the figure and north is at the top of the panel.

westward currents it appeared as if the top and bottom of the farm acted as the seabed, producing friction and, increasing shear closer to the boundaries of the farm. Shear decreased within the farm and beneath it, removing the friction effect that the seabed has on water velocities. A very similar pattern was observed with the eastward shear although here, the effect of the farm was smaller.

Although it was expected to see an undisturbed upstream shear profile, results showed similar upstream and downstream vertical profiles. This could be attributed to the M-ADCPs being close enough to the farm to perceive the flow turbulence and instability signal produced by

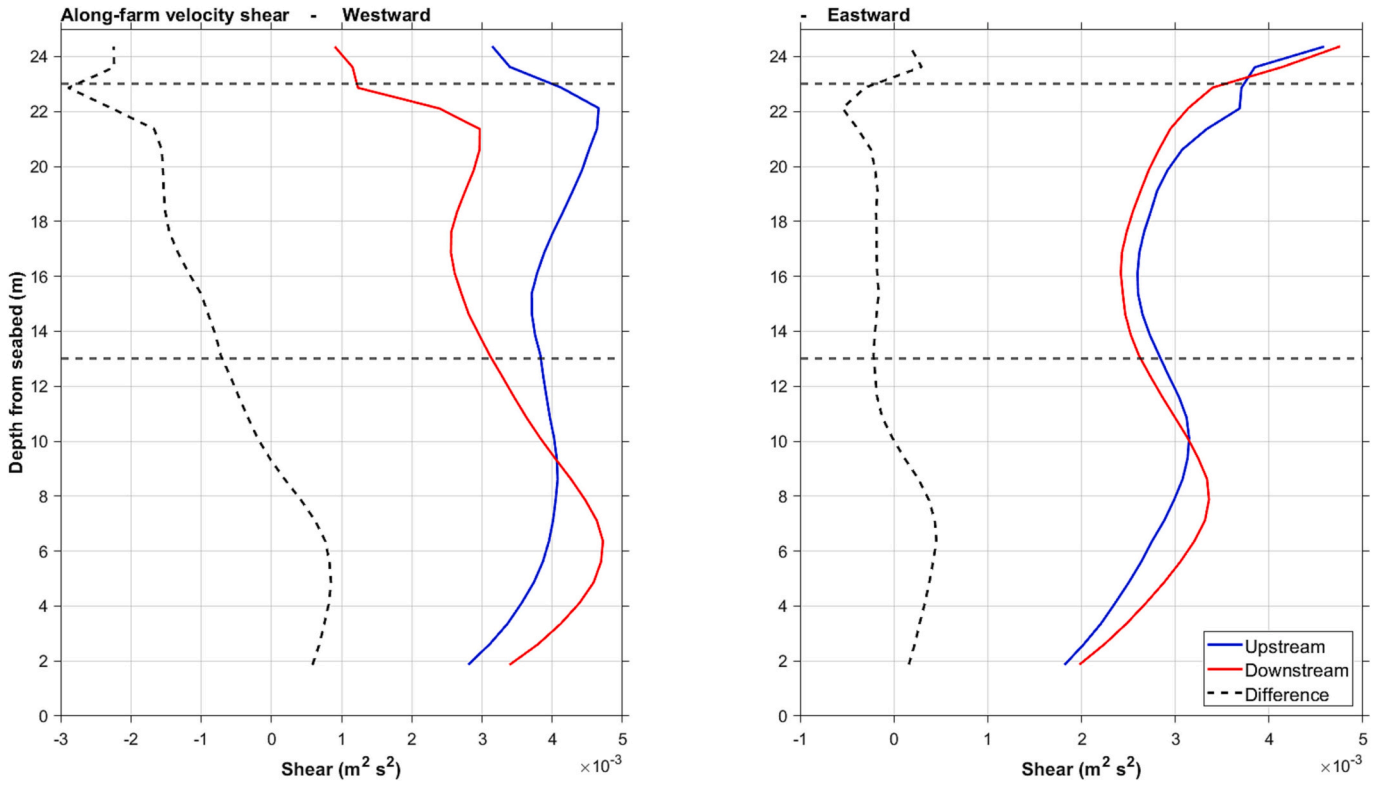

Fig. 11. Time average depth profiles of upstream and downstream shear (m^2 s^2) from two M-ADCPs over farm boundaries (horizontal grey dashed lines). Black dashed line shows differences between upstream and downstream shear.

the various changes in flow speed and direction throughout the time-series of this study.

3.2.2. *Current acceleration at the mussel farm flanks*

To assess current distortion at the flanks of the mussel farm, an entire tidal cycle VM-ADCP survey was performed. Transects were completed along the west and east sides of the farm and passed the north and south edges to study changes in current speed and direction at the farm's flanks (bottom insert, Fig. 12). Ten legs, which included both east and west transects, were performed during the 13 h survey; however, analysis was focused on two legs, Leg 2 at ebb tide and Leg 8 at flood tide (top insert, Fig. 12).

Results from depth-averaged *u* velocity analysis of Leg 2, when tidal currents were westward (HW + 1.5 h), showed upstream acceleration of the flow on the northern flank of the farm while there was deceleration on the south flank (East transect, Fig. 12). Downstream, there was an overall decrease in the westward velocity caused by the mussel farm accentuated by a strong eastward current at the north flank (West transect, Fig. 12). This could be caused by a redistribution of the flow at the downstream north edge of the farm to counteract the reduction in flow within the farm boundaries and the flow acceleration at the upstream north flank. It can be appreciated it that both upstream and downstream current profiles at the north and south of the farm are very similar however a longer transect would have been needed to further demonstrate these patterns. Overall, faster currents were recorded below the farm at depths 19–21 m and 23–24 m with the latter being the fastest. Upstream, sea surface velocities (2–4 m) were the slowest while downstream, velocity depth profiles at 2–4 m and to a lesser extent 7–9 m, were faster than those at mid-water which coincides with the bottom of the farm (12–14 m). This is in line with results above demonstrating near-seabed (Lin et al., 2016; Plew et al., 2006) and above the farm velocity increase (Fig. 2).

Results from depth-averaged *u* velocity analysis of Leg 8, when tidal currents were eastward (HW -2 h), showed an acceleration of the flow on the north and south flanks of the west (upstream) transect. This signal was not observed on the northeast and southeast flanks, which could be due to the length of both transects being shorter, potentially eluding what could have been an acceleration of the flow on the downstream flanks. It was however possible to see that, on the west of the farm, there was an area that lacked headlines (bottom inset, Fig. 12) and this could explain the eastward flow acceleration halfway through the transect on both the upstream (west) and downstream (east) sides of the farm. Downstream, there was an overall decrease in the eastward velocity were currents not only decelerated but were strongly going westward. This could be caused by the particular layout of the mussel farm headlines during the survey were most of the headlines were found on the west side of the farm and the empty space was being filled with redistributed water (bottom inset, Fig. 12).Overall, upstream currents were faster below the farm and near the seabed (19–21 m and 23–24 m) with sea surface (2–4 m) currents being the slowest as seen in Leg 2. On the contrary to the results above, downstream currents were very similar across all depths with westward flow slowest sea surface velocities but faster within-farm velocities (7–9 m).

In both legs it was clear that the farm obstructed the flow as upstream flows appeared to be blocked by the farm and were squeezed into the flanks. This is consistent with other studies that found offshore mussel farms to generate vorticity and vertical circulation at the flanks (Plew et al., 2006).

Results demonstrated that velocity changes were dependent on the different tidal phases but, particularly, on the design of the farm as well as the density and number of developed mussel headlines, which provide more or less drag, as well as the background characteristics of the area (Table 1). This farm was designed to withstand the highly hydrodynamic conditions of the area thus, headlines were highly separated from one another, suspended 3 m below the sea surface and placed in the same east-west direction to the flow, minimising the farm's drag.

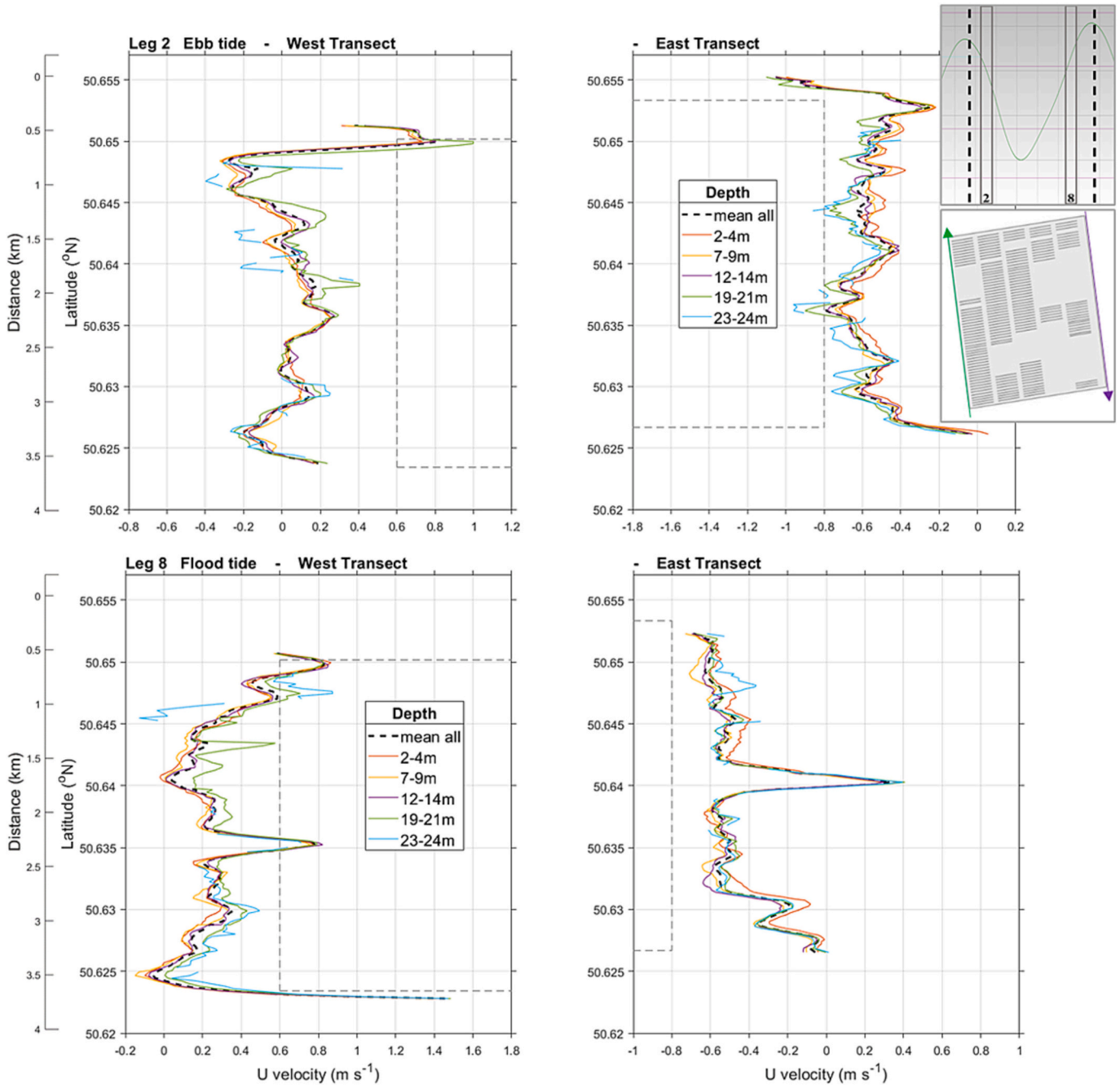

Fig. 12. Depth average U velocities along the east and west sides of the farm during Leg 2 and Leg 8 of a full tidal cycle VM-ADCP survey. Depths were chosen according to the location of the mussel farm between: the top-of-droppers (2–4 m); mid-droppers (7–9 m); bottom-of-droppers (12–14 m); below-droppers (19–21 m) and; the seabed (23–24 m). Grey dashed line represents location of the mussel farm. Leg 2 started at 10:40 (HW + 1.5 h) with westward ebb currents. Leg 8 started at 18:40 (HW-2.5 h) with eastward flood currents. Top inset shows tidal height during the VM-ADCP tidal cycle survey on 12th July 2021. Bands delimit Leg 2 and Leg 8 of the survey with black dashed lines delimiting the beginning and end of the survey. Bottom inset shows the west and east transects in respect to the mussel farm and the current headline layout of the farm during the time of the survey.

4. Conclusions

Observational data of the UK's first large scale mussel farm showed that offshore mussel farms have an impact on local current velocities. Our survey design allowed us to assess local conditions and tidal regime and successfully test our hypotheses. M-ADCPs were efficiently located allowing for comparison of upstream unaltered currents with downstream flows and were located at a distance from the farm that allowed to capture near bed accelerations, which were compromised by seabed reflection from VM-ADCP data.

This study demonstrates that suspended mussel farms like the one in Lyme Bay produce within-farm current attenuation, but this is in turn compensated by an acceleration of the flows above, beneath the ropes and around the farm's flanks. As the farm accelerated currents towards the bed, it behaves exactly the opposite to what is achieved naturally by seabed friction, which can have an impact on the ecology below and near the farm.

This study demonstrated the need for oceanographic-informed farm designs where headlines are aligned with the predominant current direction, minimising drag effect and consequent farm damage. Our

Table 1
Characteristics of three offshore suspended longline mussel farms and the results provided by the hydrodynamic studies performed for comparison with the farm under study.

Article	Location	Distance offshore (km)	Depth (m)	Years in operation	Annual production	Dimensions (km)	Number of longlines	Dropper length (m) / diameter (cm)	Total longlines	Orientation	Tide (m)	Mean current speed/ orientation
Plew et al., 2005, 2006	Collingwood, Golden Bay, South New Zealand	2.5	9–12	N/A	N/A	2.450 × 0.650	120	8/14	220	Parallel to coast N-S	4.2 m	0.119 m s^{-1}/N-S
	Main results											
	2005: 36–63% within farm current reduction. Wave attenuation of approximately 5–17%. 2006: 22–43% within farm current reduction. 60% of the flow entered the canopy: 27% of flow was diverted around and 13% diverted under. 33% of the flow was increase beneath the farm (diverted beneath) while 67% was diverted to the sides of the farm. Turbulent energy was enhanced within the canopy.											
Lin et al., 2016	Gouqi Island, East China Sea, China	Near an island >50 km from mainland	15–20	Over 10 years	78,786 tons	8 × 8	400	2.8/–	Hundreds (20 m separation)	N/A	> 2 m	1.0 m s^{-1}/ clockwise
	Main results											
	75–90% current reduction within the farm and 45% reduction at the bottom. The farm induced downwelling in the top 2/3 water column											
Mascorda-Cabre et al., 2023	Lyme Bay, Southwest UK	3–5	24–29	Since 2014	2000 tons	3 × 2	150	10/ 20–22	128	Parallel to coast *E*-W	4.4 m	0.51 ms^{-1} westward 0.36 ms^{-1} eastward/ clockwise
	Main results											
	28% within-farm current attenuation by the mussel ropes. Redistribution of flow above and under the mussel farm: 66% increase in farm surface currents at depths between 0 and 3 m and, 7% mean velocity increase under the mussel ropes. Overall increase in near-seabed velocities of 21% and 63% decrease of downstream mean sea surface velocities. 171% increase in near-seabed velocity compared to sea surface downstream of the farm. 72% reduction of through-farm surface waves. Upstream acceleration of the flow on the farm's flanks.											

observations show an effect of the farm on the local circulation, although this is perceived as minimal in comparison with circulation at a regional scale.

Having a thorough understanding of the hydrodynamics of the area is important on a range of scales and each of those important for a range of ecosystem services. Due to the novelty of such industry, this study will contribute information to further our understanding of offshore aquaculture-environment interactions. Although empirical and numerical studies on the hydrodynamic effects of mussel farms have been occurring in the last 20 years, linking those to ecological interactions is a novel field of study. Particularly, the relationship between flow modification and particle transport, resuspension of seabed material as well as understanding sedimentation rates and how these affect the ecology of the area. We recommend that further studies and, especially, field observations be performed to investigate the overall footprint extent of offshore mussel farms to obtain reliable data on the environmental impacts of such developments. This is particularly important in a context of marine spatial planning, licensing, management and, ultimately, carrying capacity of a farm's location. Considering the oceanographic conditions of an area and how these may change in accordance with a farm's design and configuration may influence whether or not the farm is successful and can produce sustainable yields.

Further studies should provide results at both local- and meso-scale levels, to assess the potential formation of a downstream wake, which would allow us to quantify the magnitude and extent of the potential ecological impact and footprint of the farm. The authors recommend that further work should focus on sediment transport using various methods and techniques such as using an Acoustic Doppler Velocimeter (ADV), a comprehensive Conductivity Temperature Data (CTD) logger, or a dye to study the pulse residence time (PRT), in combination with M- and VM-ADCP surveys. This should be performed in conjunction with a thorough ecological study, characterising not only sediments within and near the farm but the subsequent modification of macro-invertebrate communities to combine oceanographic and ecological results providing a comprehensive assessment of offshore farming effects.

Author's contributions

Experimental study was designed by LL.M-C and P·H. The article was conceived by LL.M-C with supervision by P·H, E.V·S and M.J.A. Sampling was carried out by LL.M-C and P.H. Article analysis was completed by LL.M-C with supervision by P.H. Results were discussed by LL.M-C and P.H. The manuscript was written by LL.M-C with contributions from P.H. Reviewer comments were addressed by LL.M-C with contributions from P.H, E.V·S, and M.J.A.

CRediT authorship contribution statement

Llucia Mascorda-Cabre: Writing – review & editing, Writing – original draft, Visualization, Validation, Software, Resources, Project administration, Methodology, Investigation, Formal analysis, Data curation, Conceptualization. **Emma V. Sheehan:** Supervision, Project administration, Funding acquisition, Conceptualization. **Martin J. Attrill:** Supervision, Funding acquisition. **Phil Hosegood:** Visualization, Validation, Supervision, Software, Methodology, Investigation, Funding acquisition, Formal analysis, Data curation, Conceptualization.

Declaration of competing interest

The authors declare the following financial interests/personal relationships which may be considered as potential competing interests: Prof Martin J. Attrill reports financial support was provided by Offshore Shellfish Ltd.

Dr. Phil Hosegood reports financial support was provided by Offshore Shellfish Ltd.

Dr. Llucia Mascorda-Cabre reports financial support was provided by Offshore Shellfish Ltd.

Dr. Emma V. Sheehan reports financial support was provided by Offshore Shellfish Ltd.

Data availability

Data will be made available on request.

Acknowledgements

The authors would like to thank Offshore Shellfish Ltd. for funding the PhD that has led to this article. Special thanks are given to those that helped during fieldwork, Lyme Regis fishers John Walker and Robert King. We would like to thank the anonymous reviewers for their positive feedback and valuable comments which have improved this manuscript.

Appendix A. Supplementary data

Supplementary data to this article can be found online at https://doi.org/10.1016/j.aquaculture.2024.740697.

References

Avdelas, L., Avdic-Mravlje, E., Borges Marques, A.C., Cano, S., Capelle, J.J., Carvalho, N., et al., 2021. The decline of mussel aquaculture in the European Union: causes, economic impacts and opportunities. Rev. Aquac. 13 (1), 91–118.

Cefas, 2015. Sanitary survey of Lyme Bay.Cefas report on behalf of the Food Standards Agency, to demonstrate compliance with the requirements for classification of bivalve mollusc production areas in England and Wales under EC regulation No. 854/2004. Retrieved from. https://www.cefas.co.uk/media/52799/lyme-bay-sanitary-survey-report-2015-final.pdf.

Chen, H., Liu, X., Zou, Q.-P., 2019. Wave-driven flow induced by suspended and submerged canopies. Adv. Water Resour. 123, 160–172.

EU Copernicus Marine Service, 2022. Global Ocean Hourly Sea Surface Wind and Stress from Scatterometer and Model. Retrieved from. https://data.marine.copernicus.eu/product/WIND_GLO_PHY_L4_NRT_012_004/description.

Gentry, R.R., Froehlich, H.E., Grimm, D., Kareiva, P., Parke, M., Rust, M., et al., 2017. Mapping the global potential for marine aquaculture. Nat. Ecol. Evol. 1, 1317–1324.

Giles, H., Broekhuizen, N., Bryan, K.R., Pilditch, C.A., 2009. Modelling the dispersal of biodeposits from mussel farms: the importance of simulating biodeposit erosion and decay. Aquaculture 291, 168–178.

Hondolero, D., Edwards, M.S., 2017. Changes in ecosystem engineers: the effects of kelp forest type on currents and benthic assemblages in Kachemak Bay, Alaska. Mar. Biol. 164, 81.

Kapetsky, J.M., Aguilar-Manjarrez, J., Jenness, J., 2013. A Global Assessment of Offshore Mariculture Potential from a Spatial Perspective. In: FAO Fisheries and Aquaculture Technical Paper No. 549. FAO, Rome.

Lacoste, É., Drouin, A., Weise, A.M., Archambault, P., McKindsey, C.W., 2018. Low benthic impact of an offshore mussel farm in Îles-de-la-Madeleine, eastern Canada. Aquac. Environ. Interact. 10, 473–485.

Lin, J., Li, C., Zhang, S., 2016. Hydrodynamic effect of a large offshore mussel suspended aquaculture farm. Aquaculture 451, 147–155.

Lopes, A.M., Tenreiro Machado, J.A., 2017. Tidal analysis using time-frequency signal processing and information clustering. Entropy 19 (8), 390.

Mascorda-Cabre, L., Hosegood, P., Attrill, M.J., Bridger, D., Sheehan, E.V., 2021. Offshore longline mussel farms: a review of oceanographic and ecological interactions to inform future research needs, policy and management. Rev. Aquac. 1–24.

Mascorda-Cabre, L., Hosegood, P., Attrill, M.J., Bridger, D., Sheehan, E.V., 2023. Detecting sediment recovery below an offshore longline mussel farm: a Biological Trait Analysis (BTA) of macrobenthic organisms. Mar. Pollut. Bull. 195, 11.

Matarazzo Suplicy, F., 2018. A review of the multiple benefits of mussel farming. Rev. Aquac. 12 (1), 204–223.

Pawlowicz, R., Beardsley, B., Lentz, S., 2002. Classical tidal harmonic analysis including error estimates in MATLAB using T_TIDE. Comput. Geosci. 28, 929–937.

Pereira, D., 2023. Wind Rose for Matlab. MATLAB Central File Exchange.

Plew, D.R., Stevens, C.L., Spigel, R.H., Hartstein, N.D., 2005. Hydrodynamic implications of large offshore mussel farms. IEEE J. Ocean. Eng. 30 (1), 95–108.

Plew, D.R., Spigel, R.H., Stevens, C.L., Nokes, R.I., Davidson, M.J., 2006. Stratified flow interactions with a suspended canopy. Environ. Fluid Mech. 6, 519–539.

Scridel, D., Utmar, P., Franzosini, C., Segarich, M., Menon, S., Burca, M., et al., 2020. Sink or swim? Modernization of mussel farming methods may negatively impact established seabird communities. Biol. Conserv. 243 (October 2019), 1–8.

Simon, B., Page, J. (2017). Tidal constituents. Retrieved from chrome-extension://efaidnbmnnnibpcajpcglclefindmkaj/https://flaterco.com/files/xtide/Constituents-20170508.pdf.

STECF, 2018. Scientific, technical and economic Committee for Fisheries - economic report of the EU aquaculture sector (STECF-18-19). Publ. Office Eur. Union Luxembourg 2018. ISBN 978-92-79-79402-5. Retrieved from. https://op.europa.eu/en/publication-detail/-/publication/7f9c98f0-0fe4-11e9-81b4-01aa75ed71a1.

STEFC, 2023. Scientific, Technical and Economic Committee for Fisheries (STECF) – Economic Report on the EU aquaculture (STECF-22-17). Publications Office of the European Union (Vol. Luxembourg).

Turner, J.S., 1973. Buoyancy Effects in Fluids. C. U. Press.

Zhong, W., Lin, J., Zou, Q., Wen, Y., Yang, W., Yang, G., 2022. Hydrodynamic effects of large-scale suspended mussel farms: field observations and numerical simulations. Front. Mar. Sci. 9 (August), 1–18.